

## Interfacial fracture of polymer foam-metal composites at micro-scale using finite element analysis

\*R. Das<sup>1</sup>, N. Navaranjan<sup>2</sup>, P. Browne<sup>1</sup>, G. Riley<sup>1</sup>, and C. Nguyen<sup>3</sup>

<sup>1</sup>Centre for Advanced Composite Materials, Department of Mechanical Engineering, University of Auckland, Auckland, New Zealand.

<sup>2</sup>Scion Research, Rotorua, New Zealand

<sup>3</sup>Product Accelerator, University of Auckland, Auckland, New Zealand.

\*Corresponding author r.das@auckland.ac.nz

### Abstract

Foam-metal composites are being increasingly used in a variety of applications. One important aspect in the structural integrity of foam-metal interface is the ability to resist failure around the interface whilst ensuring required load bearing capacity. This study investigated the mechanical and failure behaviour at the interface region at micro scale. The foam-metal composite consisted of polyurethane foam directly adhered to a galvanised steel face sheet. Optical, scanning electron and atomic force microscopy were used to examine the interface geometry and to obtain a realistic surface profile for use in a finite element (FE) model. Finite element analysis (FEA) was used to study the effects of different interfacial roughness profiles on mechanical interlocking and modes of failure, which are directly related to interfacial strength. A set of finite element models of idealised surface pairs of different geometries and dimensions were developed based on the microscopic observations at the foam-metal interface. The finite element modelling results show that the micro-scale roughness profile at the foam-metal interface causes mechanical interlocking and affects the stress field at the scale of the interface surface roughness, which consequently governs the specific failure mode and the relative proportion of the cohesive to adhesive failure in the interface region for a given foam-metal interface. It was found that the aspect ratio (relative width and height) and width ratio (relative spacing) of roughness elements have a significant effect on the stresses and deformations produced at the interface and consequently control the modes (cohesive or adhesive) of failure.

**Keywords:** Numerical modelling, foam, interface, fracture, cohesive fracture, adhesive fracture.

### Introduction

Sandwich composites consisting of polymer foam and metal face sheets have many advantages for structural applications. The notable benefits are light weight, high bending stiffness and strength [Grujicic et al. (2008)]. The bond between the foam and metal must remain intact to ensure the structural integrity of the composite. So optimising the adhesion strength of the interface is crucial to the performance of the composite. To effectively achieve this, it is essential to understand the mechanisms of adhesion and the effects of these on the strength of the adhesive bond [Kim et al. (2010)].

Characteristics of the interface of a solid polymer and metal have been extensively investigated. The main factors affecting the interfacial strength are chemical/physico-chemical (e.g. ionic or covalent bonds or van der Waals force) and physical (e.g. mechanical interlocking) interactions [Buehler (2008)]. Chemical interactions are related to the primary and secondary bond formations [Ho (1989); Grujicic et al. (2009)]. Mechanical interlocking is the interaction between the two material surfaces due to geometric effects [Noijen et al. (2009)] and plays a dominant role in interface bonding. A typical interlocking feature originates from the surface roughness of the interface and generally occurs at the microscopic scale. Specifically in the case of a polymer adhered directly to a metal surface, mechanical interlocking and absorption are the most significant mechanisms that contribute to the strength of the interface [Kim (2003); Grujicic et al. (2009); Kim et al. (2010); Ochoa-Putman and Vaidya (2011)]. The friction at the polymer-metal interface along with the polymer stiffness also contributes to the mechanical behaviour of the interface [Ochoa-Putman and Vaidya (2011)].

The effect of altering the surface roughness of steel at a micro-scale along with chemical treatment of the steel surface on the behaviour and strength of a steel-polymer interface [Ochoa-Putman and

Vaidya (2011)] showed that the strength of the steel-polymer interface increased as the surface roughness increased. It is suggested that the polymer-metal interfaces usually fail due to a combination of both interfacial adhesive failure between the polymer and the metal and cohesive failure of the polymer due to cracking [Yao and Qu (2002); Kim et al. (2010); Ochoa-Putman and Vaidya (2011)]. The relative strengths against cohesive and adhesive failures determine the resultant interfacial strength. For some material systems, cohesive failure typically requires more energy than that of adhesive failure; therefore interfacial strength could be improved by increasing the proportion of cohesive failure compared to adhesive one, as studied [Yao and Qu (2002)]. Altering surface roughness has been shown to result in an increase in cohesive failure and a reduction in adhesive failure [Yao and Qu (2002)], thus can increase the interfacial strength. A relationship exists between adhesive failure and the non-dimensional roughness  $\bar{R}/\lambda$ , where  $\bar{R}$  is the mean half-depth of the roughness and  $\lambda$  is the mean distance from peak to trough of the roughness (Figure 1).

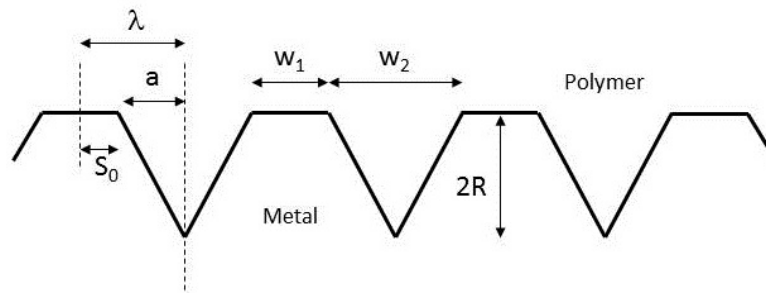


**Figure 1. Idealised profile representing surface roughness of polymer-metal interface (adapted from [Yao and Qu (2002)])**

Kim et al. [Kim et al. (2010)] also showed via a similar study that increasing the ratio of cohesive to adhesive failure along the interface is an effective way to improve the interfacial strength of a metal-polymer composite. They roughened the surface of steel with micro-line patterns and investigated the effect of varying the roughness dimensions; depth  $R$ , widths  $w_1$  and  $w_2$  and width ratio  $w_1/w_2$  (shown in Figure 1). However, changing the roughness depth  $R$  was found to have no effect on the interfacial fracture toughness. Increasing the ratio  $w_1/w_2$  resulted in a smaller fraction of area failing purely due to adhesive failure along the interface and a larger fraction of area failing due to cohesive failure of the polymer. Hence, increasing the ratio of cohesive to adhesive failure can increase the interfacial strength of several metal-polymer composites.

Numerical modelling has been successfully used to characterise polymer-metal interfaces [Yao and Qu (2002); Noijen et al. (2009)]. The finite element method (FEM) was used by Yao and Qu [Yao and Qu (2002)] to predict the energy release rate (ERR) of adhesive and cohesive cracks at different positions along a typical surface roughness profile of a metal-polymer interface. They observed that a crack along the interface propagated into the polyurethane (PU) foam when the ratio of adhesive to cohesive energy release rates ( $G_R$ ) reached a critical value.

In the numerical study by Noijen et al. [Noijen et al. (2009)], the crack was assumed to be first formed on the flat surface of the metal due to low adhesive strength, and propagated along the interface until the ERR condition along the interface and through the polymer (affected by the roughness geometry at the interface) were met, which changed the direction of crack propagation deflecting into the polymer. This was however unable to account for the relative dominance between the adhesive and cohesive failure, so an improved numerical model was deemed necessary. This work indicated that the numerical modelling can predict the location at the polymer-metal interface where the crack propagation will deviate from the interface into the polymer, which in turn enables determination of the ratio of cohesive to adhesive failure [Noijen et al. (2009)].

In this paper, we extend the previous studies on polymer-metal interface to the material system of foam-metal sandwich composite interface, namely galvanised (zinc coated) steel and polyurethane foam composite interface. It is known that polymers can adhere well to zinc coatings [Kim (2003)]. However, the key difference of foam-metal interface from that of a homogenous polymer-metal

interface is the porous and cellular structure of the foam, which affects the localised adhesive and cohesive failure mechanisms and the resulting fracture behaviour. Moreover, variability, such as temperature, polymer distribution, and poor wetting during the casting of polyurethane foam onto zinc coated steel can result in different adhesive strengths in different regions of the foam-metal interface [Kim (2003)].

Most importantly, the bulk failure behaviour at the interfacial region is manifested by micro-scale deformation and fracture patterns. To address this, the present work investigated the interface of the specific foam-metal sandwich composite made of polyurethane foam and galvanised steel face sheets at microscopic scale using experimental observations and finite element (FE) analysis. The focus was to understand how the geometry of micro-scale surface roughness influences the nature of failure at the interfacial region of the foam-metal composite. The stress-strain distributions in the micro-scale roughness profile were analysed. In the FE analyses, idealised geometries of the interface representing different surface roughness profiles were created, and the failure modes were predicted under the tensile and shear loading conditions. In the experimental study, the foam-metal sandwich samples were fabricated without using any adhesive for bonding so as to avoid any chemical effect of external adhesives. The metal-foam interface was imaged using optical and scanning electron microscopes. The surface roughness was characterised using an atomic force microscope. Subsequently, the effect of changing surface roughness parameters (i.e. aspect ratio and width ratio) on the crack propagation patterns and failure modes, and the resulting interaction between adhesive and cohesive failures were investigated using finite element analysis.

## Materials and Methods

### Material Systems

Polyurethane foam is porous, and has a cellular structure with voids. The properties of the foam can vary greatly depending on the type and proportion of the reactants used. The polyurethane foam used in this study was produced by mixing Endurathane GP38 polyol blend with Endurathane 5005 isocyanate, supplied by New Zealand Polymer Group Ltd. The stress-strain curves of the foam in tension and compression are shown in Figure 2.

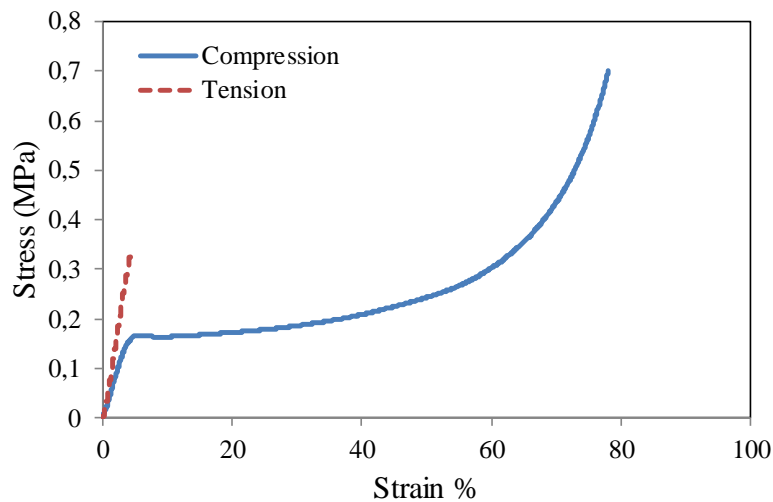


**Figure 2. Polyurethane foam stress strain curves showing the difference in behaviour when subjected to tension and compression**

A commercially available G550 galvanised high strength structural steel was used for the composite. It had a thickness of 0.75 mm. The material properties are given in Table 1. The steel surface is covered by a zinc rich layer as a result of the galvanisation. The foam contact is therefore with this zinc layer, and not with the steel. The zinc layer is significantly stiffer and stronger than the polyurethane foam (Table 1).

**Table 1. Material properties of the constituents of the foam-metal composite**

Material	Modulus of Elasticity	Yield Strength	Poisson's Ratio
Polyurethane foam [Randall and Lee (2002)]	7.5 GPa	0.34 MPa	0.40
Zinc [Davis (2014)]	83 GPa	160 MPa	0.25
G550 steel [Davis (2014)]	200 GPa	550 MPa	0.3

### *Sample Preparation*

Polyurethane foam-G550 steel sandwich composite was fabricated in a controlled laboratory condition. Composite samples that were subjected to compression tests were failed by local buckling, and foam and metal were delaminated along the interface. The foam-metal specimens were cut into approximately  $10 \times 10$  mm sections from the failed region of the samples to observe the interface failure. These specimens were used for surface roughness analysis and imaging foam cell sections. The foam-metal specimens were then moulded in an epoxy resin without causing any damage to the delaminated interface and foam (see Figure 3a). The section of each specimen was then ground and polished to obtain a smooth surface for microscopic examination. Sections of  $10 \times 10$  mm specimens were also mounted flat using double-sided carbon tape (Figure 3b) to observe the top and bottom surfaces of the failed composite.

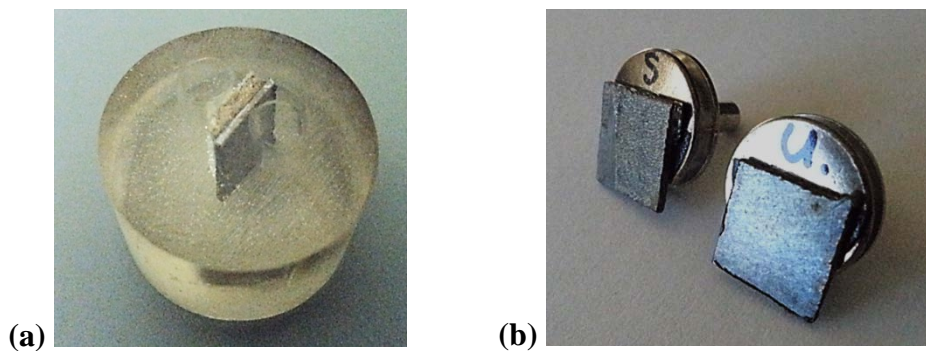


**Figure 3. (a) Specimen cross-section of foam-metal interface prepared for microscopic examination, (b) Specimens showing the top and bottom surfaces of foam-metal composite where it has failed along the interface (top specimen shows failure surface, and the bottom specimen is used as the control)**

### *Microscopic Examination*

An Olympus MX6B microscope was used to examine the prepared specimens. Dark field lighting was used, as it provides a clearer image than that of bright field lighting. The entire length of the interface was examined at 100, 200 and 500 magnification levels. Images were taken at regular intervals along the interface. Surface roughness of zinc coating was analysed using an Atomic Force Microscope.

The cross-section of the foam-metal interface, the failed surface, and the surface of steel (without foam) were observed using a Scanning Electron Microscope (SEM) at a range of magnification from  $100\times$  to  $24000\times$ . The specimens were coated with a thin platinum layer to avoid surface charge accumulation and to improve the image quality. Both the back scatter electron detector (for improved materials distinction) and secondary electron detector (for improved topography) were used to observe the specimens. Figure 4 shows a typical optical microscope image of the foam-metal interface.



**Figure 4. A typical optical microscope image of the foam-metal interface (using Dark field and 100× total magnification) showing steel (black), zinc (silver), and polyurethane foam**

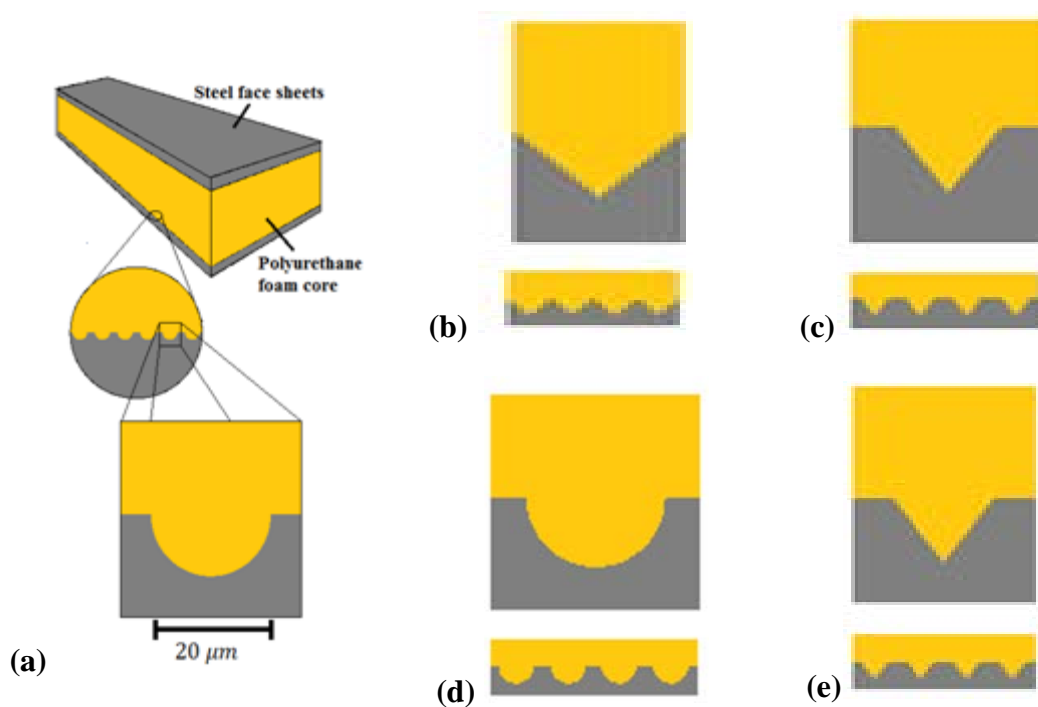


**Figure 5. Division of the foam-metal composite into individual roughness elements: (a) Foam-metal sandwich composite, micro-scale view of the foam-metal interface, and zoomed view of a typical roughness profile, (b) jagged profile, (c) triangular profile, (d) semi-circular profile, (e) Filleted triangular profile**

### Finite Element Modelling of the Interface

The foam-metal interface was modelled using FEM to understand the failure mechanisms and investigate how different roughness parameters affect the deformation behaviour and failure modes. An idealised surface roughness profile is an accurate assumption for modelling an induced roughness, especially if the technique used to induce the roughness is accurate and consistent. Even for modelling a random surface roughness (i.e. a naturally rough surface) an idealised surface roughness profile can be an accurate assumption provided it is based upon average dimensions and

a profile similar to that of the actual roughness. Idealised micro-scale surface roughness profile was modelled by dividing the foam-metal interface into individual repeating elements (RE), as shown in Figure 5. Each RE represented a roughness profile with a part of the metal and foam.

### *Materials Modelling*

A two dimensional FE model of RE was developed and analysed using the software ABAQUS [ABAQUS (2014)]. The polyurethane foam was modelled as a homogenous and isotropic solid material, as it was identified through optical microscopy that the material at the interface region was solid polyurethane rather than cellular foam (Figure 5a). The thickness of the solid film varied between 5-50  $\mu\text{m}$ . The failed interface showed that the thin solid film perfectly adhered to the metal surface (see Figure 4). Four different idealised surface roughness profiles were modelled. These are referred to as the jagged, triangular, filleted triangular and semi-circular profiles, as shown in Figure 5b-e, respectively.

Both zinc and steel are considerably stiffer and stronger than polyurethane so that it is unlikely that either will fail before polyurethane does. Hence the metal component of the interface has been modelled as analytically rigid. To simplify the analysis we have chosen to model polyurethane as behaving the same in compression as it does in tension. This is a reasonable assumption as at the micro scale solid polyurethane attached to the zinc coating is unaffected by voids that are responsible for the difference in behaviour in tension and compression at the macro scale. Figure 6 shows stress-strain curve of the polyurethane foam used in the FEA analysis.

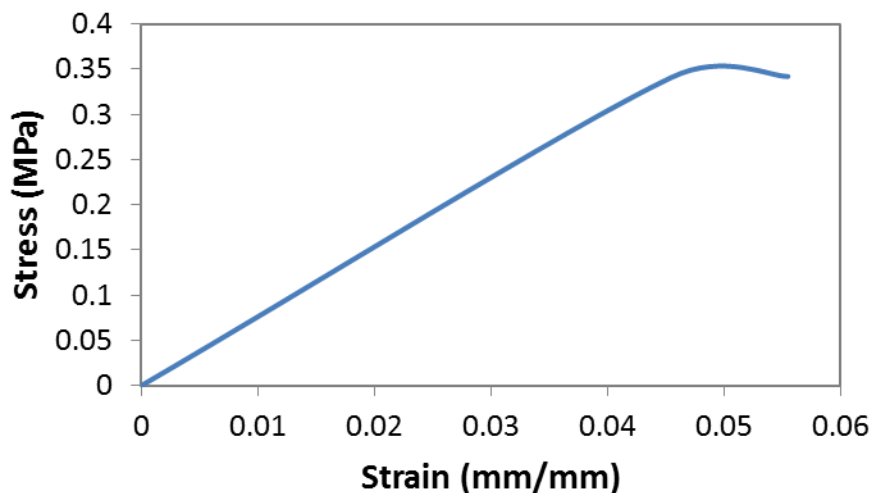


**Figure 6. Polyurethane stress-strain curve used in FEA**

### *Loading and Boundary Conditions*

The foam metal interface was analysed under two loading conditions, tension and shear loadings. So each surface roughness profile was modelled under both tensile and shear loading. The boundary conditions imposed for the tensile and shear load cases are shown in Figure 7. Both the boundary conditions included specified displacement and symmetry conditions. Each roughness element was symmetric about the vertical axis (Figure 7a). Hence, a half of the single element was modelled applying the symmetric boundary condition about the vertical axis (red lines in Figure 7b) for tensile load case. Since the foam was perfectly adhered to the zinc layer of the galvanised steel, all degrees of freedom were constrained at the foam-zinc interface in the finite element model for both load cases. This is highlighted in yellow in Figure 7b.

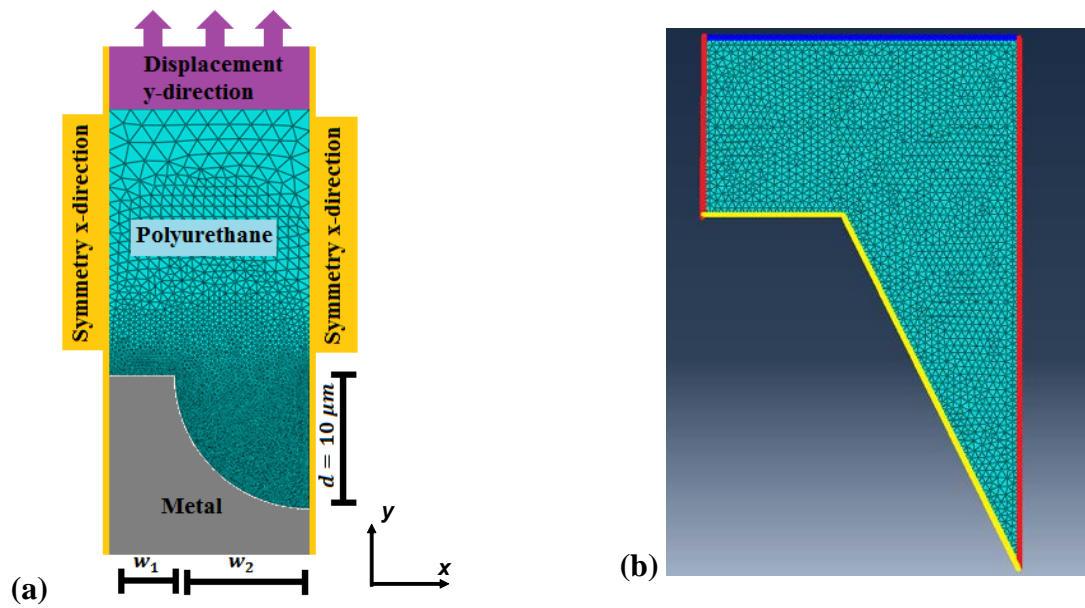


**Figure 7. Tensile boundary conditions: (a) A typical foam-metal interface model showing loads and boundary conditions for tensile loading, (b) Different boundary conditions: yellow - fixed, red - vertical (y) symmetry, blue - specified vertical displacement**

For the tensile loading, a specified displacement boundary condition of  $0.5 \mu\text{m}$  was applied to the top surface of the roughness element in the vertical direction (y-direction), which is highlighted by the blue line in Figure 7b. The direction of shear load was parallel to the horizontal interface, and as a result asymmetric loading was generated across the roughness element, implying that the symmetry boundary condition could no longer be used. Moreover, the stresses and strains generated due to shear loading were not symmetrical between adjacent roughness elements. So symmetry boundary conditions could not be used at the edge of the roughness element to compensate for the edge of the roughness element not being at a free end of the interface (see Figure 8). To account for this, the geometry used in the FE model for shear loading was a section of the metal foam interface consisting of three roughness elements, and the behaviour of the middle roughness element was evaluated. The top surface of the roughness element is displaced in the horizontal (x) direction by  $1.5 \mu\text{m}$ .

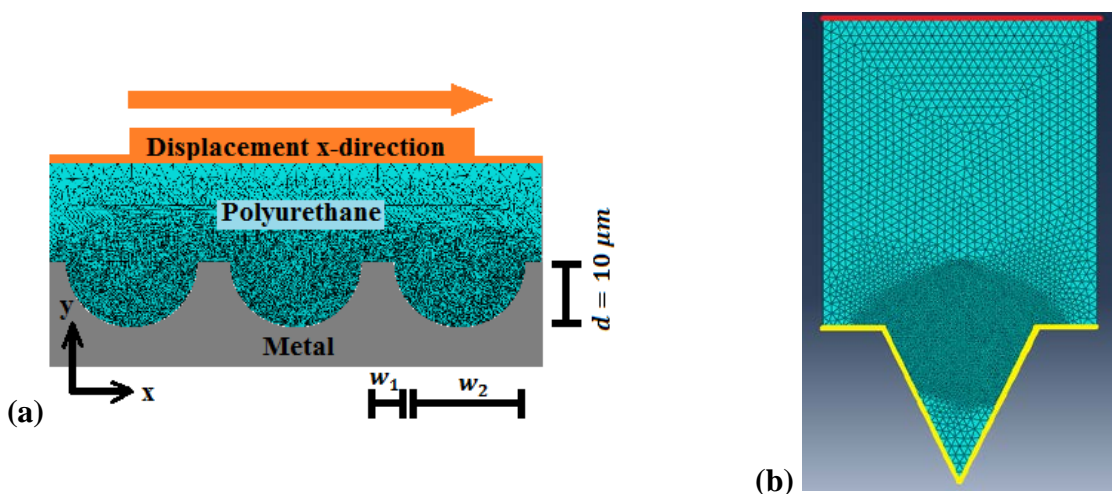


**Figure 8. Shear boundary conditions: (a) A typical foam-metal interface model consisting of three roughness elements showing loads and boundary conditions for shear loading, (b) Different boundary conditions: yellow - fixed, red - specified horizontal (x) displacement**

### Meshing and Failure Modelling

Linear 3-node triangular plain strain elements were used for all the models. The mesh was biased and was locally refined to generate fine meshes at the metal-foam interface and around the corners of the profiles in order to capture the sharp stress variation along the interface and around the corners. A finite element mesh convergence study was performed to ensure that the mesh used in the models was of sufficient resolution so as to accurately predict the stress, strain and damage evolution in the interface region.

A continuum damage model was used to model crack propagation, adopted from [Nielsen et al. (1995)]. Each element had a scalar ‘damage’ parameter  $D$  that measures its load carrying capacity. The scalar damage parameter  $D$  is used to characterise the volume-averaged micro-fracture of the volume of material represented by each element. The damage parameter is calculated based on the principal stresses of the elements. It is used to inhibit the transmission of tensile stress between elements. The damage parameter lies between 0 and 1. Material with  $D = 0$  is undamaged and is able to transmit the full tensile load, whereas material with  $D = 1$  is fully damaged and cannot transmit any tensile load, thus creating a partial macro crack. Connected macro-cracks or contiguous cracked material across a body leads to fracture. A failure criterion was used, and a material stiffness degradation model was implemented. If an element met the failure criterion, its stiffness was reduced by scaling with  $(1-D)$ .

### Microscopic Characterisation of the Interface

Figure 9 shows a surface roughness image obtained from the surface area of zinc using AFM. Figure 10 shows the cellular structure of polyurethane foam obtained from optical microscopy. At a magnification of 500, the features, such as foam pores, contact between polyurethane and zinc at the interface, distinct regions of steel, zinc and polyurethane as well as the irregularities in the zinc galvanising layer, can be observed. Figure 11 shows the solid polyurethane film (top grey) that covers the majority of the metal surface at a magnification of 8000 from SEM. The film thickness generally varies between 5-50  $\mu\text{m}$  although there are a few locations along the surface which are not covered by the film.

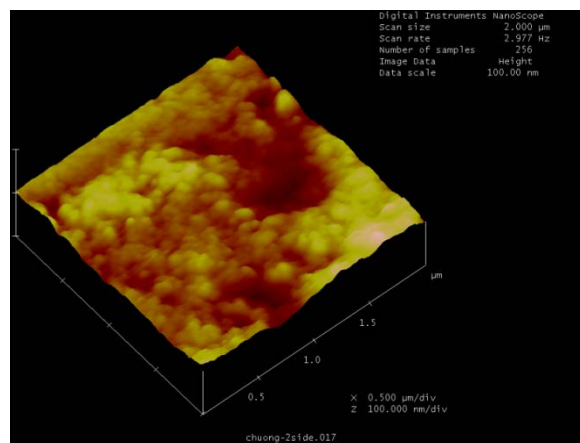


**Figure 9. Roughness profile of zinc surface of the galvanised steel**

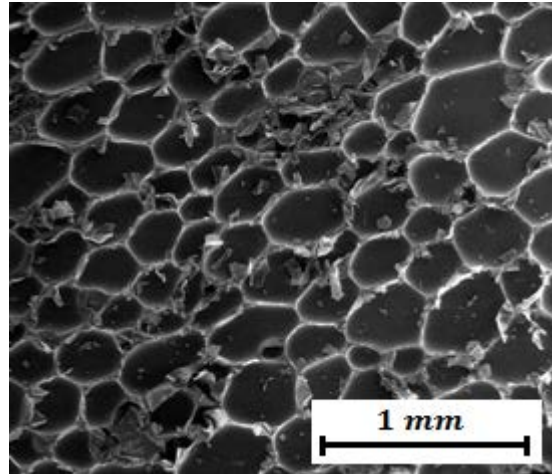


**Figure 10. Cellular structure of polyurethane foam obtained from optical microscope**

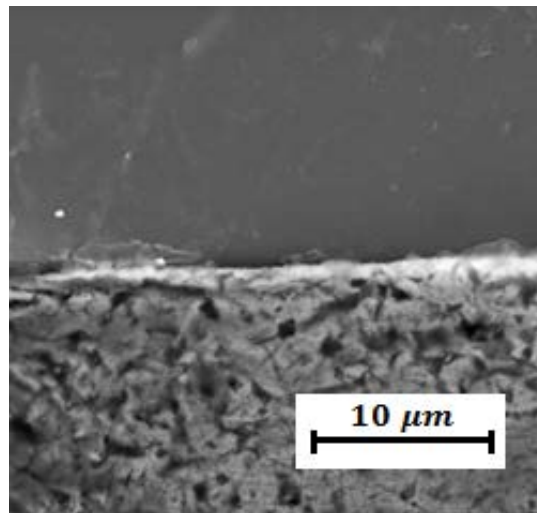
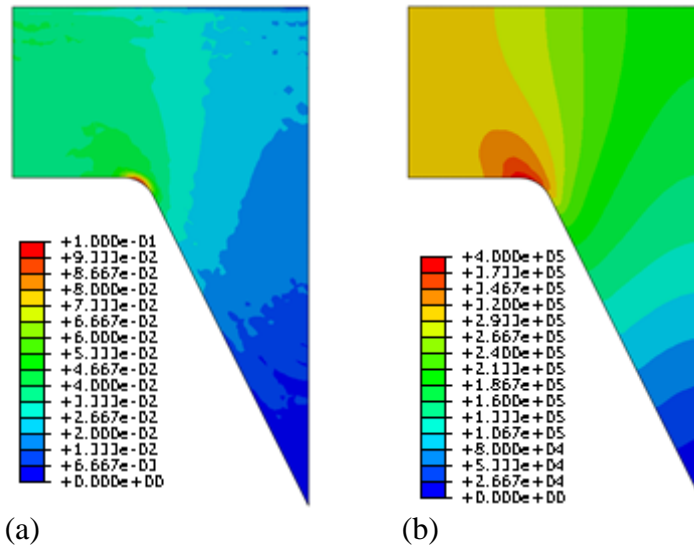


**Figure 11. SEM image showing solid polyurethane (without pores/voids) layer covering the majority of the metal surface (observed using 8000 × total magnification)**

The observations suggested that the foam-metal composite did not predominantly fail along the interface adhesively, and rather it failed near the interface by cohesive manner. The top surface specimens failed much closer to the interface than the cross-sectional specimens, i.e. in the cell walls of the cells in the vicinity of the metal surface. The stresses in the cellular area of the polyurethane foam where voids are present are considerably higher than those in the solid foam present at the foam-metal interface. This leads to the trend in cohesive failure predominantly in the cell wall as opposed to solid polyurethane. As a result of this, crack propagation due to cohesive failure would not be in the immediate vicinity of the interface. A transition from cohesive failure to adhesive failure would be unlikely due to the small area of the cell walls compared to the solid layer of polyurethane attached to the metal layer. This explains the large areas of continuous cohesive and adhesive failure zones. As a result, when the adhesive strength of the interface exceeds the cohesive strength of the polyurethane foam at a macroscopic scale (including the effect of cellular structure), the mode of failure would be exclusively cohesive in the cell walls immediately next to the interface. This limits the strength of the interface to the cohesive strength of the macroscopic polyurethane foam. If the cohesive strength of the foam on a macroscopic scale exceeds the adhesive strength of the interface, the strength of the interface would then be limited to the strength of adhesion. This study focuses on the failure that is essentially confined to the 'interface region' – the region from the metal surface up to the top of the solid polyurethane foam layer. Hence for the purpose of studying the failure modes within this interface zone, the cellular structure of the foam can be ignored.

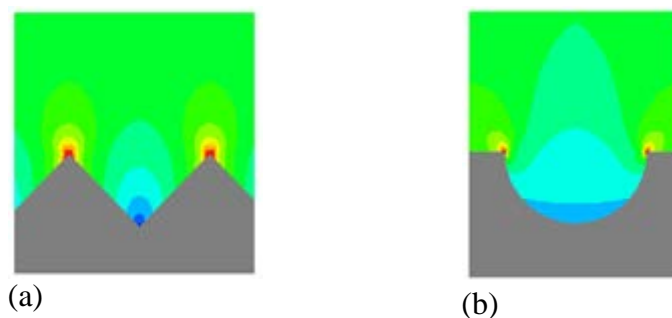
## Stress Analysis using FEM

As we focused on the solid polyurethane foam near the interface, the bulk properties of the foam was used for finite element analysis. Increasing the aspect ratio (ratio of width to height) roughness elements decreases stress concentration and reduces the likelihood of cohesive failure. Shear of the interface generally results in more adhesive failure than compared to tension (this may vary depending on material properties and adhesive strength). Typical maximum principle stress and strain distributions in a roughness element are provided in Figure 12.



**Figure 12. (a) Maximum principle strain distribution in polyurethane foam at point of yield, (b) distribution of maximum in plane stress in polyurethane at point of yield (MPa)**

Failure is initiated at points of stress concentration. The stress distribution determines the location, where polyurethane foam will first yield initiating cohesive failure. The distribution and concentration of strains at the interface between polyurethane and metal determines where adhesive failure will occur. The characteristic shape of a roughness element determines the distribution and concentration of stress and strain at the interface between the polyurethane foam and the metal. Figure 13 shows that stress distribution for roughness profiles of different shapes and how it influences the stress field and concentrations. We discuss below how a typical roughness element behaves under tensile and shear loading prior to damage or crack initiation.



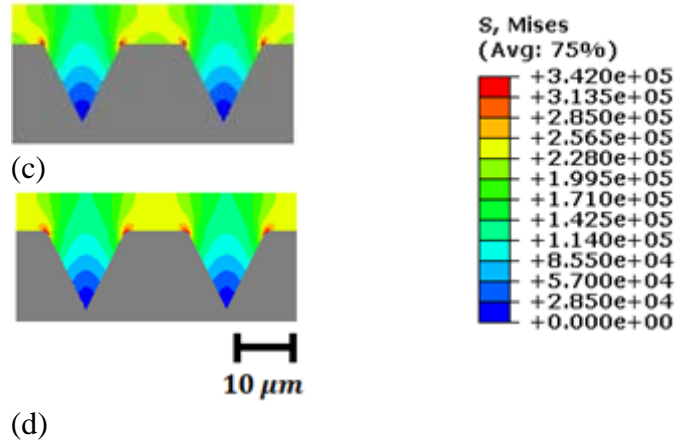
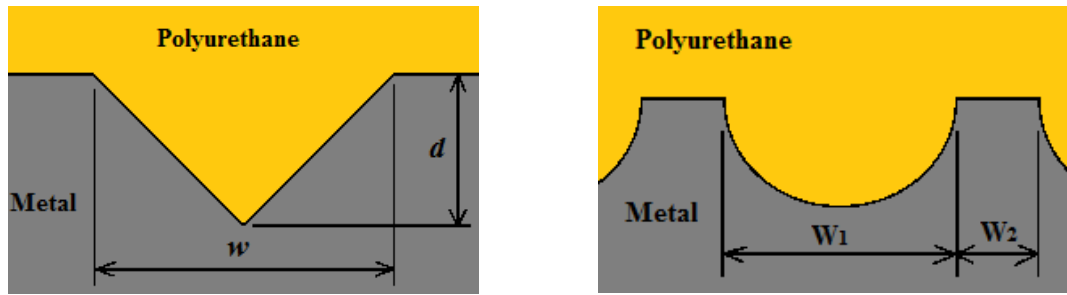


**Figure 13. von Mises Stress distribution (MPa) in the roughness profiles at point of failure for various shapes of the roughness elements; (a) Jagged, (b) Semi-circular, (c) Triangular, (d) Filleted triangular**

### Effect of Roughness Parameters on the Failure Mode

Failure is initiated at points of stress concentration. Failures which propagate along the polyurethane-steel interface will be adhesive failure and failures which propagate through the polyurethane foam will be cohesive failure. The relative magnitudes of the cohesive strength of foams and the adhesive strength of an interface govern the failure mode for a given geometry of a roughness profile and loading conditions. However, these strength values depend on the foam type, structure, processing conditions, and method of adherence to the substrate; so the exact relative proportion of cohesive and adhesive failures will depend on the specific material system. For many cases, when the adhesive strength of the interface is generally weaker than the cohesive strengths of the materials which comprise that interface, adhesive failures typically may occur before cohesive failures for foam-metal composites as cohesive failures require more energy than adhesive failures. In this case the purpose of inducing surface roughness at the foam-metal interface will be to cause cohesive failures, as a greater ratio of cohesive failure to adhesive failure will result in a stronger interface. In this study, the adhesive strength of the polyurethane steel interface and the cohesive strength of polyurethane foam were assumed to be equal, as the objective was to analysis how the geometry of the roughness profile affects the failure mechanics under different loading conditions for an interfacial region with equal strengths.

It has been identified that modifying certain roughness parameters (e.g. aspect ratio and width ratio) can improve interfacial strength by increasing the ratio of cohesive to adhesive failure around the interface ([Kim (2003); Kim et al. (2010)]). In this study we explore the effect of aspect ratio, width ratio and shape of the roughness profile on the strength and failure mechanism of foam-metal interfaces. The aspect ratio is defined as the ratio of roughness width ( $w$ ) to roughness depth ( $d$ ) as shown Figure 14a, and the width ratio is defined as the ratio of widths  $w_1$  to  $w_2$  as shown in Figure 14b. Both of these parameters have been shown to affect the strength of polymer-metal interfaces. Next the failure mechanics of roughness profiles for a range of different aspect ratios (1:1 to 4:1) and width ratios (1:1 to 8:1) will be evaluated using FEA in order to determine how they affect the interfacial failure mode.



(a) Aspect ratio,  $w:d$

(b) Width ratio,  $w_1:w_2$

**Figure 14. Definition of aspect ratio (left) and width ratio (right)**

### *Effect of Aspect Ratio*

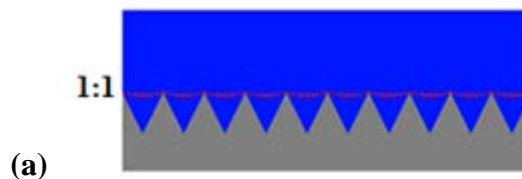
A key parameter of micro-scale roughness is the ratio of the width to the depth of the roughness elements. Increasing the aspect ratio in general reduces stress concentrations within the foam making cohesive failure less likely. Path of crack propagation is indicated by the completely damaged material, as shown by red lines in Figure 15, Figure 16, and Figure 17. Elements in red indicate where the failure criterion was satisfied, and the stiffness of corresponding elements was degraded.

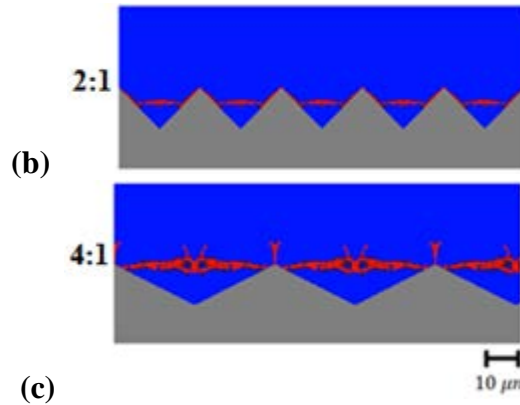
### Tensile loading

We considered ‘jagged’ roughness profiles of three different aspect ratios, viz: 1:1, 2:1, and 4:1, and analysed the crack propagation and failure modes in each case under tension (Figure 15). The crack initiated at the corners of the base of the roughness element for all the aspect ratios considered. For the 1:1 aspect ratio profile, the crack propagated exclusively through the polyurethane material between the two base corners, indicating a pure cohesive failure as shown in Figure 15a.

An increased aspect ratio of 2:1 resulted in a combination of mixed adhesive and cohesive failures (Figure 15b). The crack propagated adhesively along the interface before a cohesive failure is initiated which propagated into the polyurethane foam. For this 2:1 aspect ratio roughness profile, the cracks propagated approximately half-way down the left side of the interface of the roughness element, and then traversed across it horizontally through the polyurethane foam up to the centre, where the cracks from both the sides met. This crack pathway resulted in a failure mode which was about 50% cohesive.

For the 4:1 aspect ratio profile, the crack propagated a small distance down the interface of the roughness element, and then traversed horizontally across it through the polyurethane foam cohesively (Figure 15c). Some secondary cracking was also noticed. A second crack formed from the corner of the base of the roughness element and extended vertically into the polyurethane foam for a short distance. Two similar short cracks originated from the middle of the base and propagated upwards following slightly inclined paths. So a higher aspect ratio again leads to predominant cohesive failure with localised secondary fracture.

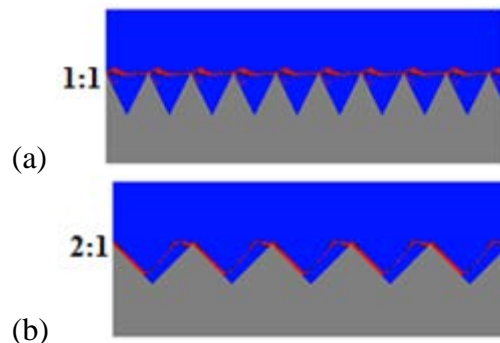




**Figure 15. Jagged roughness profile in tension, showing fracture paths for different aspect ratios**

### Shear loading

We considered roughness profiles of the same aspect ratios as before, and analysed the crack propagation and failure mode in each case under shear. The cracks paths are shown in Figure 16. Under shear loading for all of the aspect ratios considered, the crack propagation initiated from the left corner of the roughness element. For the 1:1 aspect ratio case, two crack paths were formed (Figure 16a). The main crack propagated from the left side of the roughness element to the other side causing fracture. This caused a nearly pure cohesive failure. A secondary crack was also created from the left corner and propagated a short distance down the roughness profile nearly parallel to the interface of the roughness element. For the case with an aspect ratio of 2:1, the failure mode changed to partly adhesive and partly cohesive (Figure 16b). Only one crack path was present in this case. This crack path extended nearly three quarters of the way down the left face of the roughness element interface causing adhesive failure. Then the crack traversed across the roughness element, moving diagonally up to the top of the roughness element and across to the right corner causing cohesive fracture. The crack path for the 4:1 aspect ratio profile was similar to that of the 2:1 aspect ratio profile with a larger adhesive failure component (Figure 16c). The crack propagated downwards along the left surface of the roughness element up to approximately 90 percent of the left interface. Then it turned upwards and traversed through the polyurethane foam, but remained close to the right interface, before reaching the upper right corner. This shows a combination of adhesive and cohesive failures in the left and right interfaces for the roughness profile with a high aspect ratio. Overall, as the aspect ratio of the roughness profile increases, the proportion of adhesive failure increases under shear. This study was repeated for the triangular profile and similar trends in the transition in behaviour from cohesive to adhesive failure was noticed, as shown in Figure 17.



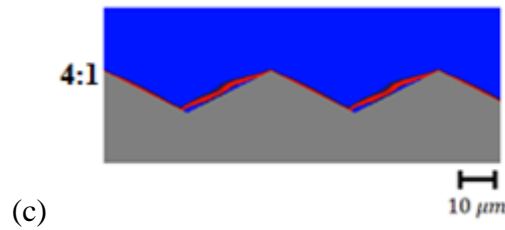


**Figure 16. Jagged roughness profile in shear, showing fracture paths for different aspect ratios**

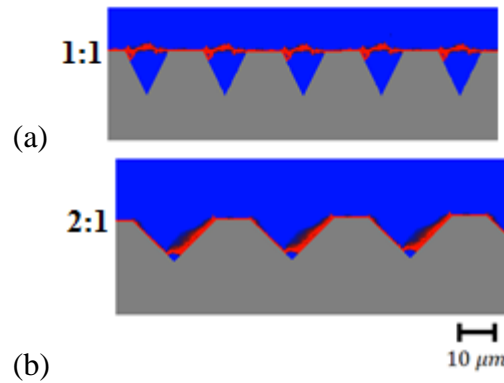


**Figure 17. Triangular roughness profile in shear, showing fracture paths for different aspect ratios**

#### *Effect of Width Ratio*

One characteristic feature of surface roughness is the relative spacing between adjacent roughness elements. We studied the effect of this by investigating the effect of width ratio on the fracture pattern. In this case, we considered a semi-circular roughness profile so as to be different from that considered in the aspect ratio case.

#### Tensile loading

For this study, we considered three width ratios, 1:1, 3:1, and 8:1, for the semi-circular roughness profile. The fracture paths for the primary (major) cracks of the semi-circular roughness profile in tension are nearly the same for all width ratios (Figure 18). For all three width ratios modelled under tensile load, the primary cracks are initiated from the two corners of the base of each roughness element, where the stress concentrations occur. From each corner, two primary cracks are initiated and propagated in the reverse direction. One of them propagated along the flat part of the interface first adhesively, and another one propagated cohesively into the polyurethane foam. The two cohesive cracks met at the centre of each roughness element.

However, secondary cracks and local level of damage for the three width ratios are somewhat different. For the 1:1 width ratio roughness profile, the two cohesive cracks met at the centre, and then extended upward into the body of the polyurethane (Figure 18a). The cracks generated in the 3:1 width ratio roughness profile caused larger damage as it propagated across the base of the roughness element (Figure 18b). The localised cracks from the centre are smaller in length and damage at the middle of the base is large. The 8:1 width ratio roughness profile showed a crack path similar to that of the 3:1 width ratio model (Figure 18c); however, the crack paths was thinner, and it produced less damage as it propagated across the base of the semi-circular roughness element.

A roughness profile of 1:1 width ratio results in approximately 50% cohesive failure, a 3:1 width ratio in 75% cohesive failure, and a 8:1 width ratio in 89% cohesive failure. From the width ratios considered, the 8:1 width ratio produces the largest cohesive failure due to it having the smallest width ' $w_2$ '.

Broadly, within a roughness element, the width ratio does not significantly affect the mode of failure. Adhesive failure in the flat portion and cohesive failure within the roughness elements are observed in general with some difference in crack paths, due to the loading direction and the presence of stress raisers (corners). However, width ratio has a direct effect on the strength of an interface by altering the proportion of cohesive and adhesive failure. As noticed in the semi-circular surface profile under tension, when the width ratio decreases the proportion of the horizontal flat surface at the interface decreases, given the length of the roughness element base remains constant. The crack propagated across the base of the roughness elements for all of the width ratios; so decreasing the width ratio reduced the area where adhesive failure could occur, thus increasing the proportion of the cohesive failure zone.

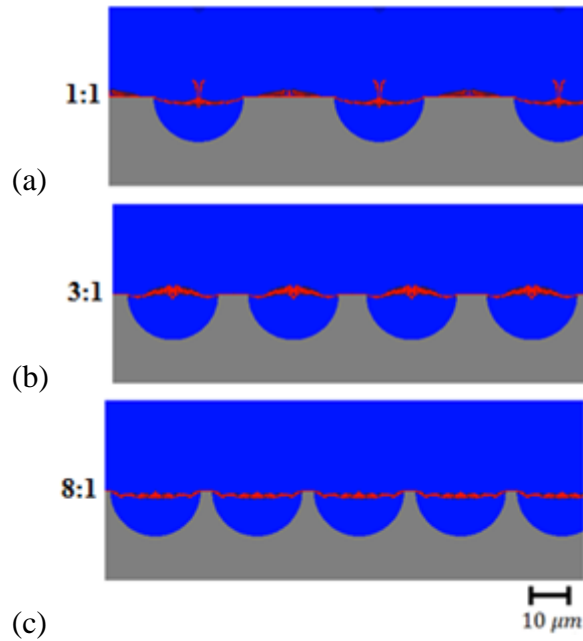


**Figure 18. Semi-circular profile in tension showing failure paths for width ratios of 1:1, 3:1, and 8:1.**

#### Shear loading

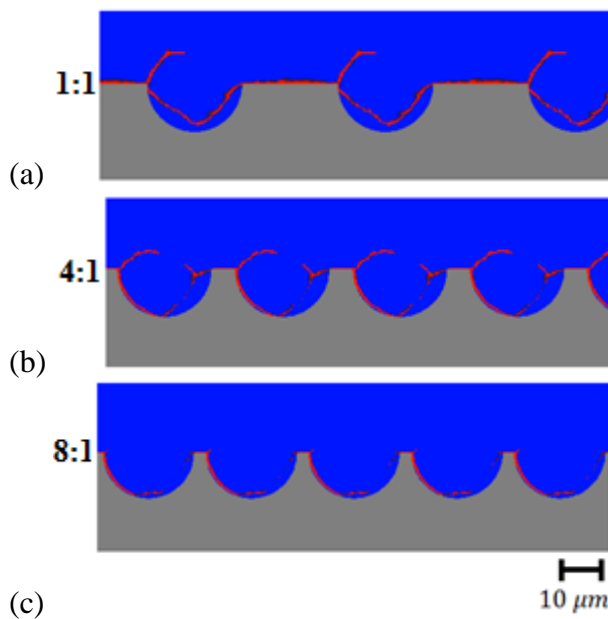
Next we study the effect of the width ratio on the failure mode under shear by considering a semi-circular roughness profile. Three different width ratios from low to high values, 1:1, 4:1 and 8:1, were adopted. Figure 19 shows the fracture pattern under shear loading for various width ratios of the roughness profile. For all of the width ratios modelled, the crack initiated from the left side and first propagated along the flat interface, thus causing adhesive failure. Upon reaching the left corner where the semi-circular profile met the flat face, the crack behaviour depended on the width ratio of the roughness profile.

Figure 19 shows the fracture pattern for the 1:1 width ratio profile. When the tip of the crack reached the left corner of the roughness element, the crack divided into branches to produce two cracks. Both the cracks subsequently traversed cohesively within the foam. The first crack propagated downwards across the roughness element in an inclined direction. Before reaching the interface, it turned about  $45^\circ$  to move in the upward direction to reach the right corner of the roughness element. The second crack initiated from the left corner, propagated into the body of the polyurethane foam in an inclined upward direction (approximately  $45^\circ$ ) up to about  $10\ \mu\text{m}$ , and then bent towards right to traverse horizontally for a short length.

The crack path for the 4:1 width ratio profile had some features similar to that of the 1:1 width ratio profile (Figure 19b). The key differences are that the first crack propagated along the interface following the circular boundary, causing adhesive failure of the interface that continued up to nearly the bottom point of the roughness element. The crack then diverted upwards into the foam, and propagated across the roughness element in a curved path to reach the right corner. Another crack

branched out from this ‘first’ crack just before reaching the right corner. A second crack also originated from the left corner for this case. This crack propagated upwards in a curved path, causing cohesive failure of the polyurethane foam, similar to the 1:1 width ratio case. For the 8:1 width ratio roughness profile, the crack path followed the left hand semi-circular interface of the roughness element up to the bottom point (Figure 19c). This crack produced a fracture that primarily occurred along the interface in the roughness element, signifying a pure adhesive failure.

Hence for the 1:1 width ratio profile, the polyurethane foam fails cohesively within the semi-circular roughness elements, although the failure follows a path closer to the interface. For the roughness profiles with 4:1 and 8:1 width ratios, the failure progressively changes from cohesive to adhesive, with partial adhesive failure for the 4:1 width ratio profile and complete adhesive failure for the 8:1 width ratio profile.



**Figure 19. Semi-circular profile in shear showing failure paths for width ratios of 1:1, 4:1, and 8:1**

## Conclusions

In this study, the interface of a polyurethane foam and galvanised steel composite was examined using optical microscopy, SEM, and AFM. A micro-scale finite element model was subsequently developed to analyse the effect of interface roughness on the mode of failure under tension and shear. It was found that whilst the macroscopic properties of polyurethane foam are affected by voids, the microscopic properties of polyurethane at the foam-metal interface are not affected considerably, because a thin film of solid (void-less) polyurethane effectively covers the majority of the surface of the galvanised steel. Thus, the macroscopic properties of polyurethane foam including the effect of voids are not good representation of the micro-scale properties of polyurethane at the foam-metal interface.

Both the relative width to depth of roughness elements and the spacing between roughness elements, as characterised by the aspect ratio and width ratio, respectively, were found to have a profound influence on the mode of failure and interfacial strength. Cohesive failure was the dominant mode of failure in the roughness profiles under tensile load irrespective of the aspect ratio as anticipated. It was found that under tension the roughness profiles with a lower aspect ratio would fail with a large proportion in a cohesive manner when compared to the higher aspect ratios of the same roughness profile. Based on the results of the present analysis, the jagged roughness profile with a 1:1 aspect ratio leads to almost pure cohesive failure. With a moderate aspect ratio of 2:1, the failure mode changes to a combination of partly adhesive and partly cohesive modes, whilst a further increase in the aspect ratio (4:1) leads to predominant cohesive failure mode again. Failure mode under shear strongly depends on the aspect ratio of the roughness profile. For low aspect ratio

roughness, the failure is primarily cohesive, which then transitions to a combination of adhesive and cohesive failures with an increase in the aspect ratio.

Under tensile loading, adhesive failure in the horizontal flat portion and cohesive failure within the roughness elements are observed, in general, for all width ratios with some local differences in the crack paths. This is due to the direction of loading combined with the stress concentration generated at the corner of the roughness element.

When a roughness profile is subjected to shear (for the semi-circular shape in this case), the cohesive failure mainly occurs when the width ratio is low. However, for higher width ratios, the failure no longer propagates cohesively in the polyurethane, but instead propagates partially or completely adhesively along the interface. For example, for a width ratio of 8:1, a pure adhesive failure of the interface occurs.

Controlling interface roughness can change the relative proportion of cohesive and adhesive failures at a foam-metal interface, which in turn can improve the interfacial strength of a foam-metal composite based on the difference between the cohesive strength of the foam and the adhesive strength of the interface. For example, if the cohesive strength is greater than the adhesive strength, then the jagged surface roughness profile with a 1:1 aspect ratio is the optimum surface roughness profile as it results in approximately pure cohesive failure when loaded either in tension or in shear.

The approach adopted in this paper to evaluate the effect of roughness parameters on the failure mode around the interfacial region can be extended to other polymer-metal composites. Future work will be undertaken to determine micro-scale adhesive strength of polyurethane and galvanised steel for specified foam-metal composites to provide accurate model input. It appears that the key aspect to improve the strength of a foam-metal composite interfacial region is to enable preferred failure modes (cohesive/adhesive) by inducing controlled micro-scale roughness profiles accurately and consistently on the surface of the metal substrate [Kim et al. (2010)], which can be accomplished using mechanical (micro machining) and/or chemical (photochemical machining) methods.

## Acknowledgement

The authors would like to acknowledge the support of Materials Accelerator Program, New Zealand for this work.

## References

- ABAQUS (2014) ABAQUS Documentation, Dassault Systems, Providence, RI, USA.
- Buehler, M. J. (2008) Atomistic Modeling of Materials Failure, Springer, New York.
- Davis, J. R. (2014) Metals Handbook Desk Edition, ASM International, Materials Park, OH, USA.
- Grujicic, M., Sellappan, V., Kotrika, S., Arakere, G., Obieglo, A., Erdmann, M. and Holzleitner, J. (2009) Suitability analysis of a polymer-metal hybrid technology based on high-strength steels and direct polymer-to-metal adhesion for use in load-bearing automotive body-in-white applications, *Journal of Materials Processing Technology* **209**, 1877-1890.
- Grujicic, M., Sellappan, V., Omar, M. A., Seyr, N., Obieglo, A., Erdmann, M. and Holzleitner, J. (2008) An overview of the polymer-to-metal direct-adhesion hybrid technologies for load-bearing automotive components, *Journal of Materials Processing Technology* **197**, 363-373.
- Ho, P. S. (1989) Chemistry and adhesion of metal-polymer interfaces, *Applied Surface Science* **41-42**, 559-566.
- Kim, J. R., E. Miller, J. Bai, J. (2003) Adhesion of a rigid polyurethane foam to zinc phosphated steel, *Journal of Adhesion Science and Technology*.
- Kim, W.-S., Yun, I.-H., Lee, J.-J. and Jung, H.-T. (2010) Evaluation of mechanical interlock effect on adhesion strength of polymer-metal interfaces using micro-patterned surface topography, *International Journal of Adhesion and Adhesives* **30**, 408-417.
- Neilsen, M., Krieg, R. and Schreyer, H. (1995) A constitutive theory for rigid polyurethane foam, *Polymer Engineering and Science* **35**, 387-394.
- Noijen, S. P. M., van der Sluis, O., Timmermans, P. H. M. and Zhang, G. Q. (2009) Numerical prediction of failure paths at a roughened metal/polymer interface, *Microelectronics Reliability* **49**, 1315-1318.
- Ochoa-Putman, C. and Vaidya, U. K. (2011) Mechanisms of interfacial adhesion in metal-polymer composites – Effect of chemical treatment, *Composites Part A: Applied Science and Manufacturing* **42**, 906-915.

Randall, D. and Lee, S. (2002) *The Polyurethanes Book*, Wiley, New York.

Yao, Q. and Qu, J. (2002) Interfacial versus cohesive failure on polymer-metal interfaces in electronic packaging - Effects of interface roughness, *Journal of Electronic Packaging* **124**, 127-134.